



Nuclear Features of the Fusion Ignition Research Experiment (FIRE)

M.E. Sawan, H.Y. Khater, S.J. Zinkle

April 2002

UWFDM-1175

Presented at the 6th International Symposium on Fusion Nuclear Technology, 7–12 April
2002, San Diego CA

FUSION TECHNOLOGY INSTITUTE

UNIVERSITY OF WISCONSIN

MADISON WISCONSIN

DISCLAIMER

This report was prepared as an account of work sponsored by an agency of the United States Government. Neither the United States Government, nor any agency thereof, nor any of their employees, makes any warranty, express or implied, or assumes any legal liability or responsibility for the accuracy, completeness, or usefulness of any information, apparatus, product, or process disclosed, or represents that its use would not infringe privately owned rights. Reference herein to any specific commercial product, process, or service by trade name, trademark, manufacturer, or otherwise, does not necessarily constitute or imply its endorsement, recommendation, or favoring by the United States Government or any agency thereof. The views and opinions of authors expressed herein do not necessarily state or reflect those of the United States Government or any agency thereof.

**Nuclear Features of the Fusion Ignition
Research Experiment (FIRE)**

M.E. Sawan, H.Y. Khater, S.J. Zinkle*

Fusion Technology Institute
University of Wisconsin
1500 Engineering Drive
Madison, WI 53706

April 2002

UWFDM-1175

*Oak Ridge National Laboratory, Oak Ridge, TN 37831

Presented at the 6th International Symposium on Fusion Nuclear Technology, 7–12 April 2002,
San Diego CA.

Abstract

The main nuclear features of the baseline design of FIRE have been evaluated. Critical issues were addressed and R&D needs were identified. Modest values of nuclear heating occur in the FIRE components. The total nuclear heating in the 16 TF coils during DT shots is 19 MW. The cumulative damage in the copper alloys used is very low (< 0.05 dpa). However, issues of low temperature embrittlement and thermal creep at high temperatures need to be resolved by an R&D program. The radiation induced resistivity increase in the conductors of the TF coils is primarily due to displacement damage and is $< 20\%$ of the unirradiated resistivity. The magnet insulator development R&D program should involve irradiation to dose levels up to 1.5×10^{10} Rads with the proper mix between neutrons and gamma photons (50% gamma dose) relevant to FIRE conditions. Low levels of activity and decay heat are obtained. Hands-on ex-vessel maintenance is feasible. All components qualify as Class C low-level waste. Activation of nitrogen gas inside the cryostat produces a very small amount of ^{13}N and ^{14}C .

1. Introduction

The Fusion Ignition Research Experiment (FIRE) is in the preconceptual design phase. It utilizes 16 cryogenically cooled wedged copper TF coils with beryllium copper in the inner legs and OFHC copper in the outer legs [1]. The baseline design has a major radius of 2.14 m and an aspect ratio of 3.6. Pulses producing a total of 5 TJ of DT fusion energy and 0.5 TJ of DD fusion energy are planned. The average neutron wall loading during the 150 MW DT pulses with widths up to 20 s is 2.25 MW/m². A double walled vacuum vessel (VV) with integral shielding has been adopted with thickness varying from 5 cm in the inboard (IB) side to 54 cm in the outboard (OB) side. The VV consists of 1.5 cm thick inner and outer facesheets made of 316SS with 60% 304SS and 40% water shield between them. The plasma facing components (PFC) include Be coated Cu first wall (FW) and divertor plates made of tungsten rods mounted on a water-cooled Cu heat sink.

Nuclear analysis has been performed to evaluate the impact of design options and assess if the major performance objectives of the project can be met. The neutronics and shielding calculations were performed using the ONEDANT module of the DANTSYS 3.0 discrete ordinates particle transport code system [2] and the activation analysis was performed using the DKR-PULSAR2.0 activation code system [3]. The most recent FENDL-2 nuclear evaluated data was used. Both the IB and OB regions were modeled simultaneously to account for the toroidal effects. The machine is assumed to have an operation schedule of four pulses per day with 3 hours between pulses. The impact of different FW/tile design options on the nuclear parameters was assessed [4]. The FW/tile design chosen consists of 0.5 cm Be PFC, 1.8 cm CuCrZr tiles and 0.2 cm gasket (50% Cu). A 2.5 cm water-cooled CuCrZr (15% water) VV cladding is employed behind the tiles. The nuclear performance parameters were determined for the different components of the baseline design [5]. In this paper, we summarize the main nuclear features of the FIRE baseline design. In addition, more thorough analyses of several critical issues are given with identification of R&D needs.

2. Nuclear heating

Nuclear heating deposited in the different components was determined for the DT pulses with the largest fusion power of 150 MW. Table 1 gives the peak power density values in the different components at the chamber midplane. Figure 1 gives the nuclear heating distribution in the OB FW/tiles at midplane. Nuclear heating in the VV drops by an order of magnitude in ~ 18 cm. The largest power density values in the magnet occur in the IB region at midplane. Calculations were also performed for the outer divertor which is exposed to the most severe conditions in the divertor region.

Table 1. Peak nuclear heating (W/cm³) at midplane.

	IB	OB
Be PFC	25.0	26.7
Cu Tiles	35.2	34.7
Cu VV Cladding	30.2	30.1
H ₂ O Cladding Coolant	20.7	23.2
SS Inner VV Wall	25.4	23.2
SS VV Filler	24.7	21.4
H ₂ O VV Coolant	11.2	11.6
SS Outer VV Wall	22.7	0.053
Cu Magnet	14.6	0.014

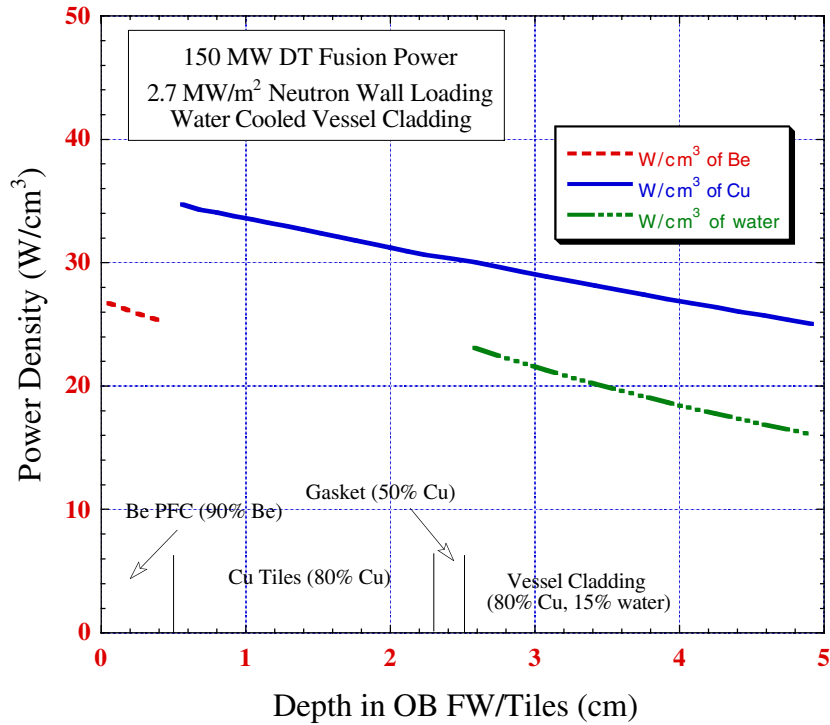


Fig. 1. Nuclear heating distribution in the OB FW/tiles.

The results revealed that relatively high nuclear heating of 37 W/cm^3 is deposited in the W rods with a peak value of only 13 W/cm^3 in the Cu heat sink. The amount of nuclear heating in the TF magnets strongly influences the achievable pulse length. Nuclear heating in the IB magnet drops by an order of magnitude in $\sim 28 \text{ cm}$. The total nuclear heating in the 16 TF coils during the DT shots is 19 MW with 90% of it deposited in the lightly shielded IB legs. For the DD pulses with the largest fusion power (1 MW), nuclear heating values are at least two orders of magnitude lower.

3. Vacuum vessel radiation damage

Since the VV is protected from the fusion neutrons by the thin FW/tiles, the issue of reweldability was addressed. The end-of-life helium production in the VV structure should be limited to 1 appm to allow for rewelding. This is the limit used in ITER [6]. For the FIRE goal of cumulative 5 TJ DT and 0.5 TJ DD fusion energy, the peak VV He production values in the IB, OB, and divertor regions are 0.11, 0.15, and 0.016 appm, respectively. The contribution from DD shots is very small ($< 0.15\%$). The results imply that reweldability of the VV should not be a concern.

4. Copper radiation damage

Table 2 gives the end-of-life peak dpa values in the Cu tiles, VV cladding, Cu heat sink in outer divertor, and Cu TF coils for the FIRE baseline design. Although the damage levels are very low, significant effects on physical and mechanical properties might occur. These effects are strongly

Table 2. Peak end-of-life Cu dpa in FIRE.

	Total dpa
IB Tiles	0.0327
OB Tiles	0.0359
Divertor	0.0150
IB VV Cladding	0.0215
OB VV Cladding	0.0246
Magnet at IB	0.00666
Magnet at OB	7.54×10^{-6}
Magnet at Divertor	4.55×10^{-4}

dependent on irradiation temperature and have been the subject of numerous studies as part of the ITER R&D program [7].

Low-temperature radiation embrittlement at $T < 150^{\circ}\text{C}$ is a concern for Cu alloys with reductions in tensile ductility (uniform elongation) below 5% being observed for damage levels on the order of 0.01 dpa. However, the fracture toughness is typically maintained at a sufficiently high level, at least in precipitation hardened alloys such as CuCrZr and CuNiBe. It is possible to maintain the high tensile ductility by periodically annealing the Cu at $\sim 300^{\circ}\text{C}$ for ~ 50 hr. Irradiation to ITER doses of 1-10 dpa at higher temperatures showed a pronounced increase in the uniform elongation of CuCrZr compared with irradiation at lower temperatures. However, at $T > 300^{\circ}\text{C}$ this is accompanied by significant softening. This was demonstrated by about an order of magnitude loss of yield strength at about 300°C for 2-10 dpa.

Void swelling takes place in copper alloys irradiated in the temperature range of 180 to 530°C . While void swelling is pronounced in copper containing oxygen impurities ($\sim 2.5\%/dpa$), it is only $\sim 0.5\%/dpa$ in pure Cu and is generally insignificant in Cu alloys up to doses of 60 dpa. Therefore, for the low dose levels in FIRE, void swelling is not a concern. The effect of irradiation on the creep of Cu alloys is uncertain due to limited data. The extremely low doses expected in FIRE reduce the importance of irradiation creep. The magnitude of the irradiation creep can be estimated using the creep compliance coefficient B. Using a conservative B value of $\sim 3 \times 10^{-6} \text{ MPa}^{-1} dpa^{-1}$ and the peak cumulative dpa value in FIRE (0.036 dpa), the irradiation creep for an applied stress of 100 MPa would amount to a total deformation of only 10^{-5} (0.001%) at end-of-life in FIRE. It was recommended [7] that the operation temperature of high strength Cu alloys should be limited to $< 300^{\circ}\text{C}$ for applied stresses of 100-200 MPa to have tolerable irradiation and thermal creep at ITER conditions of 1-10 dpa. The thermal creep strength begins to decrease rapidly for temperatures $> 300^{\circ}\text{C}$. This might cause deformation in the Cu during extended operation (> 100 hr) at 300°C . Due to the low doses in FIRE significant deformation from irradiation creep is not anticipated. Some thermal creep deformation in Cu alloys might occur if operated at elevated temperatures ($> 300^{\circ}\text{C}$). There is a lack of detailed studies on fatigue, fracture toughness and fatigue crack growth rate behavior in high-strength, high-conductivity copper alloys [8,9].

The Cu alloys operate at different temperatures in the FIRE components. The tiles can get to temperatures over 400°C . The tiles carry no primary stresses and should be basically unloaded except for thermal stresses and disruptions. Therefore, problems with high-temperature softening and creep should not be of concern. In addition, the tiles can be easily replaced if needed. The temperature of the VV Cu cladding is lower than 250°C . At this peak temperature, occurring at midplane, the low-temperature embrittlement for CuCrZr is not an issue. That will be a concern only for the lower

temperature parts of the cladding at the top and bottom of the chamber. However, the dpa level will also be lower at these locations resulting in alleviating the embrittlement concern. We also have the option of annealing out the copper damage if we bake the vessel to $> 300^{\circ}\text{C}$. The Cu in the divertor will have peak temperatures close to 500°C . The peak damage level is only 0.015 dpa. The issue here will be mainly thermal creep. The temperature of the TF coils rises from 80 to 373 K during each pulse. The main issue here is the low-temperature embrittlement. The low temperature embrittlement data on CuNiBe and OFHC Cu are limited to tensile tests between room temperature and 100°C [10]. The concern is primarily at the IB midplane where the peak damage rate is ~ 0.007 dpa, which is at the lower range of damage for the occurrence of radiation embrittlement. Much lower damage levels occur at other locations of the TF coil.

Based on the irradiation levels and operation conditions in FIRE and the available data on Cu alloys, we can identify the R&D needs as follows:

- Data on loss of ductility of BeCu (or OFHC) at temperatures between 80 and 373 K with doses < 0.01 dpa.
- Data on fatigue, fracture toughness and fatigue crack growth rate behavior in high-strength, high-conductivity copper alloys.
- Thermal creep data for CuCrZr at temperatures up to 500°C . There is no need to perform irradiation creep measurements on Cu alloys for the low doses proposed in FIRE.

5. Radiation induced resistivity in the copper conductors of the TF coils

The 17510 BeCu alloy is used in the inner legs of the TF coils with 10200 OFHC copper being utilized in the rest of the TF coils. A concern with Cu magnet conductors is the increased electrical resistivity that impacts the performance of the TF coils through increasing the I^2R heating and re-distributing the current across the coil. The temperature at the end of the pulse will increase with possible impact on the achievable pulse length. The increase in electrical resistivity results from solute transmutation products and displacement damage. In a low fluence machine like FIRE resistivity increase is dominated by point defects and defect clusters produced by displacement damage.

The solute transmutation component of resistivity increase is directly proportional to the solute content. We calculated the concentration of transmutation products accumulating at the end-of-life as a function of position in the TF coils. The BeCu alloy includes 1.8% Ni and 0.4% Be and the transmutation products are dominated by Ni, Zn, Co, Fe, and H. The worst conditions for the BeCu occur in the IB leg at midplane where the peak cumulative dpa is 0.0067. For the OFHC copper, the worst conditions are behind the divertor at the top/bottom of the machine where the peak cumulative dpa is 4.6×10^{-4} . Table 3 gives the peak concentration of the transmutation products at these poloidal locations. The Ni included in the unirradiated BeCu transmutes at a rate comparable to the production rate of Ni from Cu resulting in negligible net production of Ni. Fe is produced from the transmutation of Ni. The resistivity increases associated with these concentrations were calculated using the solute resistivities of 1.12, 0.3, 6.4, 9.3, and 1.5 $\text{p}\Omega\text{-m/appm}$ for Ni, Zn, Co, Fe, and H, respectively [8]. The results are given in Table 3. Due to the high mobility of hydrogen in copper at room temperature, it diffuses out of the material as the magnets heat up at the end of each pulse. Thermal annealing is not expected to cause any changes in the resistivity increase contributed by the other solute transmutation products. Therefore, the largest resistivity increase from transmutation effects is 0.943 $\text{p}\Omega\text{-m}$ in the

Table 3. Peak resistivity increase from solute transmutation products at different locations of TF coils at end-of-life.

Solute	Peak solute concentration (appm)		Peak resistivity increase (pΩ-m)	
	BeCu alloy IB midplane	OFHC copper behind divertor	BeCu alloy IB midplane	OFHC copper behind divertor
Ni	0	0.1044	0	0.1169
Zn	1.930	0.0712	0.579	0.0214
Co	0.041	0.0017	0.262	0.0109
Fe	0.011	0	0.102	0
H	0.315	0.0177	0.473	0.0266

BeCu alloy and 0.149 pΩ-m in the OFHC copper. These values are much smaller than the unirradiated resistivities in the temperature range of the FIRE magnets. In addition, the neutron flux drops as one moves deeper in the magnet resulting in decreasing transmutations and lower resistivity increase.

An analytical formula given by Eq. 1 [11] can be used to estimate the resistivity increase due to displacement damage for copper and Cu alloys. At high doses the displacement damage component approaches a constant saturation value due to displacement cascade overlap effects. The recommended value of the parameter B is 100 for both BeCu and OFHC copper under FIRE operating conditions [12]. The parameter A represents the saturation resistivity. Based on electrical resistivity measurements, the expected saturation resistivity increase for pure Cu irradiated near room temperature is 1.2 nΩ-m [13]. Higher resistivity increases have been measured for Hycon CuNiBe [8] due to partial dissolution of precipitates by displacement cascades, which injects solute into the copper matrix. Based on available experimental data, we used saturation values (parameter A in Eq. 1) of 1.2 and 4.2 nΩ-m for OFHC and BeCu, respectively. These include the effect of annealing during the pulse as the magnet warms up.

$$\Delta\rho \sim A[1-e^{-B \cdot \text{dpa}}] \quad (1)$$

Periodic annealing of the copper components at temperatures well above recovery Stage V (~ 425 K, corresponding to thermal dissociation of vacancy clusters [14]) would cause a significant additional reduction in the displacement damage component of the resistivity increase beyond that already achieved at room temperature. It is speculated that up to ~ 90% of the displacement damage component of the resistivity increase present in Cu specimens irradiated near room temperature could be recovered by annealing near 573 K [12]. Hence, if the magnets of FIRE can be baked-out to temperatures above 200°C (preferably 300°C), we can significantly reduce the resistivity increase. We made the conservative assumption that such bake-out is not employed.

Using Eq. 1 along with the cumulative atomic displacement values, we determined the largest increase in BeCu resistivity to be 2.05 nΩ-m in the inner leg at midplane. The largest increase in OFHC copper resistivity is only 0.05 nΩ-m behind the divertor at the top/bottom of the machine. Notice that these resistivity increases occur during pulses near the end of the machine's life. Early in

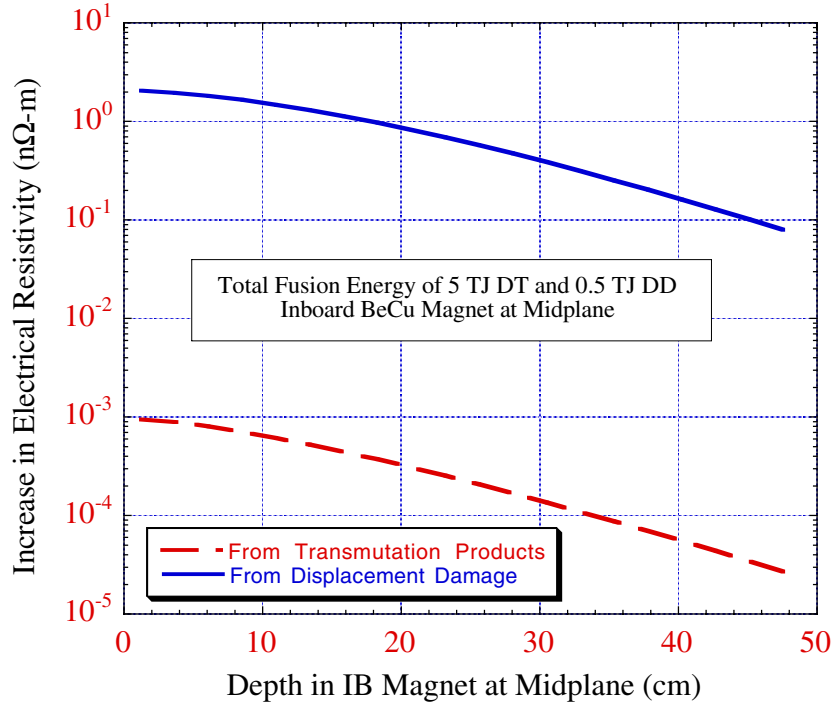


Fig. 2. Resistivity change in BeCu as a function of depth in magnet at inboard midplane.

the life of the machine, the accumulated dpa is very low and the resistivity increase is much lower. In addition, the resistivity increase drops as one moves from the plasma side of the coil deeper in the magnet.

Figure 2 shows the resistivity increases at end-of-life from solute transmutation products and displacement damage in the BeCu alloy as a function of depth in the inner leg of the TF magnet at midplane. It is clear that the total resistivity increase is dominated by displacement damage with the resistivity increase from solute transmutation products contributing less than 0.05% of the total resistivity increase. The resistivity increase drops by a factor of ~ 30 across the magnet thickness. Resistivity increase from solute transmutation products contributes less than 0.3% of the total resistivity increase of the OFHC copper conductor. The spatial distribution of the resistivity results in re-distributing the current across the coil.

The unirradiated resistivity of the 68% IACS BeCu used in FIRE varies from ~ 10 nΩ-m at 80 K to ~ 30 nΩ-m at room temperature [15]. This implies that the maximum increase in resistivity of the BeCu at end-of-life varies from $\sim 20\%$ at the start of the pulse to $\sim 7\%$ at the end of the pulse. The unirradiated resistivity of the 10200 OFHC copper used in FIRE ranges from ~ 2 nΩ-m at 80 K to ~ 16 nΩ-m at room temperature [15]. Hence, the maximum increase in resistivity of the OFHC copper at end-of-life varies from $\sim 2.5\%$ at the start of the pulse to $\sim 0.3\%$ at the end of the pulse. The unirradiated resistivities given above are without applied magnetic field. Magnetoresistance effects can lead to significant resistivity increase at cryogenic temperatures of up to a factor of 10 depending on the magnetic field and Cu purity [16]. However, much smaller magnetoresistivity increases occur in copper components operating at the higher temperatures of FIRE. The largest magnetoresistivity effects occur in the inner leg. For the peak magnetic field of 15 tesla the peak magnetoresistivity increase in the BeCu is $\sim 7\%$ at the start of the pulse and drops to $\sim 2\%$ at the end of the pulse when

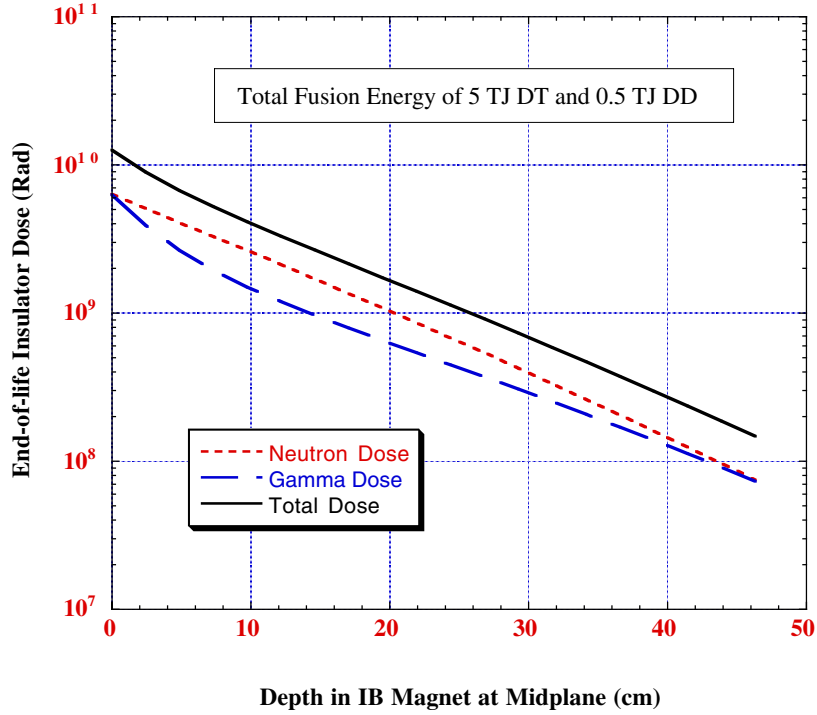


Fig. 3. Radial variation of insulator dose in the IB magnet.

the magnet heats up. The magnetoresistivity effects also decrease as one moves deeper in the inner leg of the coil due to the decreasing magnetic field. These increases are the same during all pulses over the life of the machine. The magnetoresistivity effects are lower than those resulting from irradiation effects during pulses at the end of the machine life. However, during pulses early in the life of the machine magnetoresistivity effects yield resistivity increases larger than those resulting from irradiation effects.

6. Magnet insulator dose

The insulator dose rate in the TF magnet was calculated at the front layer of the magnet winding pack. The peak cumulative magnet insulator dose is 1.26×10^{10} in the lightly shielded IB leg at midplane. At this location the fast neutron fluence ($E > 0.1$ MeV) is 9.8×10^{18} n/cm² and the total neutron fluence is 1.8×10^{19} n/cm². About 55% of the neutron fluence is above 0.1 MeV at the front of the magnet and drops to 35% at the back of the magnet. The DD shots contribute 13% of this value. The dose rate decreases by three orders of magnitude as one moves poloidally to the OB midplane. The relative DD contribution decreases as one moves poloidally from the IB midplane to only 1.6% at the OB midplane. The insulator dose decreases as one moves radially from the front to the back of the winding pack as shown in Figure 3. The gamma contribution to the total dose is 35-50%. The dose decreases by an order of magnitude in ~ 22 cm of the IB magnet.

The mechanical strength, dielectric strength, and electric resistivity are the important properties that could be affected by irradiation. The shear strength is the property most sensitive to irradiation. The commonly accepted dose limit for epoxies is 10^9 Rads. This is the limit used in ITER [10]. Polyimides and bismaleimides are more radiation resistant with experimental data showing only a

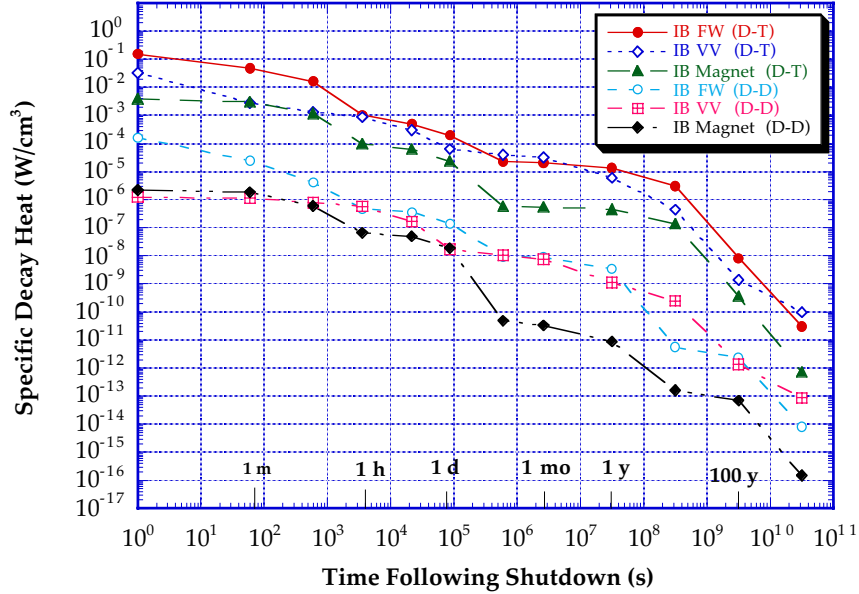


Fig. 4. Decay heat induced in the inboard side.

small degradation in shear strength at dose levels in excess of 10^{10} Rads. However, they are difficult and expensive to process due to their high viscosity and requirement for high temperatures to fully cure. In addition, they have initial mechanical properties lower than those achievable with epoxies. Hybrids of epoxies, polyimides, bismaleimides, and cyanate esters are being developed to both improve the insulation system's ability to withstand high levels of radiation and to improve the resin system's overall processibility [16]. That includes irradiation measurements at dose levels close to those expected in FIRE [17]. The information provided here gives guidance to the insulator development R&D program regarding the dose levels and the proper mix between neutron and gamma irradiation to insure relevance to the FIRE conditions.

In the FIRE design with wedged coils and added compression ring, the TF inner leg insulation does not have to have significant bond shear strength, which is most sensitive to radiation. The peak torsional shear stresses occur at the top and bottom of the IB leg behind the divertor. The end-of-life insulator dose at these locations is reduced to $\sim 10^9$ Rads due to the additional shielding provided by the divertor. Based on that, it is expected that insulation materials will be identified that can last for the whole device lifetime with the proposed operation scenario and load conditions.

7. Activity and decay heat

Figure 4 shows the specific decay heat values generated in the IB region. The PFC on the FW and divertor produce the highest levels of specific activity and decay heat. However, the operational schedule with several hours between pulses allows for the decay of short-lived radionuclides between pulses, resulting in low levels of activity and decay heat at shutdown. Immediately following DT shots, the largest specific activity is ~ 100 Ci/cm³ and the largest specific decay heat is ~ 0.2 W/cm³. The activity and decay heat generated following DD shots are at least three orders of magnitude lower. The decay heat induced in the FW/tiles, divertor, and Cu magnet at shutdown is dominated by the copper isotopes ^{62}Cu ($T_{1/2} = 9.74$ min) and ^{66}Cu ($T_{1/2} = 5.1$ min). The decay heat induced in the VV at shutdown is dominated by the ^{52}V ($T_{1/2} = 3.76$ min) and ^{56}Mn ($T_{1/2} = 2.578$ hr) isotopes. In general,

the short-term activity and decay heat values at shutdown are almost fully dominated by activation during the last pulse.

8. Biological dose rates

In order to assess the feasibility of hands-on maintenance, biological dose rates were calculated. The biological dose rates behind the VV remain significantly higher than the 2.5 mrem/hr required for hands-on maintenance for several years following DT shots. Following DD shots, the dose rates are five orders of magnitude lower than after DT shots allowing for hands-on maintenance. The dose rates behind the magnet at midplane are acceptable for both DD and DT shots. Neutron streaming through the large midplane ports results in excessive dose rates. Our results indicate that using a 110 cm thick steel shield plug in these ports will provide adequate shielding that allows for hands-on maintenance. In addition, the analysis indicated that a 20 cm thick shield placed above the TF coils results in an acceptable dose at the top of the machine. Both the midplane port plug and the top shield were included in the FIRE baseline design to allow for hands-on ex-vessel maintenance.

9. Routine release of ^{13}N to the environment

Liquid nitrogen is used to cool the magnets between shots. As a result, nitrogen gas will exist inside the cryostat during the shots and will get irradiated. One radiological concern is the generation of ^{13}N that is a major source of radioactive hazard. Activation calculations were performed for nitrogen gas at room temperature for different locations inside the machine. The activation of nitrogen gas during the D-T shots will produce ^{13}N as well as a small amount of ^{14}C . Table 4 gives the amount of ^{13}N and ^{14}C generated at different locations inside the cryostat following each D-T shot. The results indicate that the largest amount of ^{13}N and ^{14}C is generated in the space between the IB magnet and the IB VV. This is due to the fact that the shield thickness on the IB side is much smaller than that on the OB side leading to exposing the nitrogen gas in the IB region to a larger and harder neutron flux. Although the gas volume in the IB side is smaller than in the OB side, the total activity is still about two orders of magnitude larger. Notice that the ^{13}N and ^{14}C activity generated is very small since the high density liquid nitrogen does not exist in the magnet during the pulses. Another source of radioactive ^{13}N is the activated air inside the building (outside the cryostat). The amount of ^{13}N generated in the air per D-T shot is only 2×10^{-7} Ci. In addition, air activation results in generating 6×10^{-11} and 2.1×10^{-6} Ci of ^{14}C and ^{41}Ar per D-T shot, respectively. These are extremely low levels of activity and should not cause any radiological concern. Since ^{13}N has a short half-life of 9.97 minutes, the option of designing a nitrogen-holding system that allows for a significant decay of ^{13}N before releasing it to the environment is adopted in FIRE.

10. Waste disposal ratings (WDR)

The radwaste classification of the different components of the machine was evaluated according to both the NRC 10CFR61 [18] and Fetter [19] waste disposal concentration limits. At the end of the machine life, all components would qualify for disposal as Class C low level waste. The IB FW has the largest WDR value of 0.2. According to Fetter limits, the WDR values are dominated by the silver impurities in the CuCrZr alloy and the niobium impurities in the 316SS and 304SS alloys. The 10CFR61 limits indicate that the WDR values of components made of the CuCrZr alloy are dominated by ^{63}Ni which is produced from copper by the (n,p) reaction. On the other hand, the WDR values of components made of the steel alloys are dominated by their niobium impurities.

11. Summary

The main nuclear features of the baseline design of FIRE have been evaluated. Critical issues were addressed and R&D needs were identified. Modest values of nuclear heating occur in the FIRE components. The amount of nuclear heating in the TF magnets strongly influences the achievable pulse length. The total nuclear heating in the 16 TF coils during DT shots is 19 MW. End-of-life He production values imply that the VV will be reweldable. The cumulative damage in the copper alloys used is very low (< 0.05 dpa). The issues that need to be resolved by an R&D program include low temperature embrittlement and thermal creep at high temperatures. In addition, data on fracture toughness and fatigue crack growth rate behavior in the copper alloys are needed. The radiation induced resistivity increase in the conductors of the TF coils is primarily due to displacement damage. This resistivity increase is 7-20% of the unirradiated resistivity for the BeCu alloy used in the inner legs and 0.3-2.5% for the OFHC copper used in the rest of the coils. Magnet insulators with radiation tolerance up to $\sim 1.5 \times 10^{10}$ Rads are being developed. The insulator development R&D program should involve irradiation to dose levels with the proper mix between neutrons and gamma photons (50% gamma dose) relevant to FIRE conditions.

The operational schedule with several hours between pulses allows for the decay of short-lived radionuclides between pulses, resulting in low levels of activity and decay heat at shutdown. Following DT shots hands-on ex-vessel maintenance is possible with the 110 cm shield plug in midplane ports and the 20 cm shield at the top of the TF coils. All components will qualify as Class C low-level waste. Nitrogen gas will exist inside the cryostat during shots and will get irradiated. Following a DT pulse, the activities of ^{13}N and ^{14}C are only 0.9 and 1.3×10^{-6} Ci, respectively. A nitrogen-holding system will be utilized to allow for significant decay of ^{13}N before releasing it to the environment.

Acknowledgement

Support for this work was provided by the U.S. Department of Energy.

References

- [1] D. Meade, "Fusion ignition research experiment (FIRE)," *Fusion Technology*, vol. 39, p. 336, 2001.
- [2] R. Alcouffe et al., "DANTSYS 3.0, One-, two-, and three-dimensional multigroup discrete ordinates transport code system," RSICC Computer Code Collection CCC-547, Contributed by Los Alamos National Lab, August 1995.
- [3] M. Sisolak, Q. Wang, H. Khater and D. Henderson, "DKR-PULSAR2.0: A radioactivity calculation code that includes pulsed/intermittent operation," unpublished.
- [4] M. Sawan and H. Khater, "Nuclear analysis of the FIRE ignition device," *Fusion Technology*, vol. 39, p. 393, 2001.
- [5] M. Sawan and H. Khater, "Nuclear considerations for FIRE," 19th IEEE/NPSS SOFE Meeting, Atlantic City, NJ, USA, January 22-25, 2002.

- [6] Technical Basis for the ITER Final Design Report, Cost Review and Safety Analysis, ITER EDA Documentation Series, IAEA, Vienna, December 1997.
- [7] S. Fabritsiev, S. Zinkle, and B. Singh, "Evaluation of copper alloys for fusion divertor and first wall components," *Journal of Nuclear Materials*, vol. 233-237, pp. 127-137, 1996.
- [8] S.J. Zinkle and S.A. Fabritsiev, "Copper alloys for high heat flux structure applications," *Atomic and Plasma-Material Interaction Data for Fusion, Supplement to Nuclear Fusion*, vol. 5, pp. 163-192, 1994.
- [9] D.J. Alexander, S.J. Zinkle and A.F. Rowcliffe, "Fracture toughness of copper-base alloys for fusion energy applications," *J. Nucl. Mater.*, vol. 271&272, pp. 429-434, 1999.
- [10] S.J. Zinkle and W.S. Eatherly, "Tensile and electrical properties of unirradiated and irradiated Hycon 3HP CuNiBe," *Fusion Materials Semiannual Progress Report for Period Ending June 30, 1996, DOE/ER-0313/20*, Oak Ridge National Lab, pp. 207-216, 1996.
- [11] G. Burger, H. Meissner, and W. Schilling, *Physica Status Solidi*, vol. 4, p. 281, 1964.
- [12] S.J. Zinkle, ORNL, private communications, October 2001.
- [13] S.J. Zinkle, Electrical resistivity of small dislocation loops in irradiated copper, *J. Phys. F: Met. Phys.*, vol. 18, pp. 377-391, 1988.
- [14] S.J. Zinkle, Fundamental radiation effects parameters in metals and ceramics, *Radiat. Eff. Def. Solids*, vol. 148, pp. 447-477, 1999.
- [15] P. Titus, MIT Plasma Science and Fusion Center, private communications, December 2001.
- [16] P. Fabian, et al., "Highly radiation-resistant vacuum impregnation resin systems for fusion magnet insulation," *Proc. International Cryogenic Materials Conference*, July 16-20, 2001, Madison, Wisconsin, USA.
- [17] K. Bittner-Rohrhofer, et al., "Characterization of reactor irradiated organic hybrid insulation systems for fusion magnets," *Proc. International Cryogenic Materials Conference*, July 16-20, 2001, Madison, Wisconsin, USA.
- [18] Nuclear Regulatory Commission, 10CFR part 61, "Licensing requirements for land disposal of radioactive waste," *Federal Register*, FR 47, 57446, 1982.
- [19] S. Fetter, E. Cheng, and F. Mann, "Long term radioactive waste from fusion reactors," *Fusion Engineering and Design*, vol. 13, pp. 239-246, 1990.